

# Dynamical analysis of the effect of elliptically polarized laser pulses on molecular alignment and orientation

Jingsong Liu (刘劲松), Qiyuan Cheng (程起元), Daguang Yue (岳大光),  
Xucong Zhou (周旭聪), and Qingtian Meng (孟庆田)\*

*School of Physics and Electronics, Shandong Normal University, Jinan 250358, China*

*\*Corresponding author: qtmeng@sdsu.edu.cn*

Received June 26, 2018; accepted August 27, 2018; posted online September 20, 2018

In this Letter, we study the molecular alignment and orientation driven by two elliptically polarized laser pulses. It is shown that the field-free molecular alignment can be achieved in a three-dimensional (3D) case, while the field-free molecular orientation is only along the  $x$  and  $y$  directions, and that the field-free alignment and orientation along different axes are related to the populations of the rotational states. It is demonstrated that changing the elliptic parameter is efficient for controlling both in-pulse and post-pulse molecular alignment and orientation. The delay time also has an influence on the field-free molecular alignment and orientation.

*OCIS codes:* 320.5390, 020.1670.

*doi:* 10.3788/COL201816.103201.

In recent decades, with the development of laser technology, dynamical analysis of laser-controlled molecular alignment and orientation has attracted much attention due to its significance in chemical reactions, high-order harmonic generation, multiphoton ionization, surface processing, and so on<sup>[1–10]</sup>. For a linear polar molecule, molecular alignment means that the molecular axis is along the pulse polarization direction, while the molecular orientation is based on the alignment and points to a specific direction.

Earlier methods to align and orient molecules include using a dc electric field through the permanent dipole interaction<sup>[11,12]</sup>. Later, researchers found that using the dc electric field combined with a non-resonant laser pulse can obtain a higher degree of alignment or orientation<sup>[13]</sup>. However, the strong dc field can easily induce Stark effect in real applications, so it cannot be widely used and replaced by various laser pulses. Up to now, there are many kinds of laser techniques to achieve alignment and orientation both in experiment and theory, such as the two-color and multi-color laser pulse<sup>[14–17]</sup>, the single-cycle or few-cycle terahertz (THz) laser pulse and the combination of different pulses<sup>[18–24]</sup>. The related studies showed that the laser intensity, pulse duration, pulse shape, and pulse delay, as well as the temperature of the system, have a significant effect on the molecular alignment and orientation. Based on the different pulse durations, two different molecular alignment and orientation dynamic regimes were found, i.e., adiabatic and non-adiabatic regimes of alignment and orientation<sup>[25–27]</sup>. For the former case, in which the pulse duration is long compared to the rotational period of the molecule, a pendular state is created, and the molecular ensemble evolves along it. The latter case, also named field-free molecular alignment and orientation, shows an opposite situation, which can be viewed as a rapid “kick” to drive the molecular axis

toward the laser field direction, and after the pulse, the alignment and orientation can be repeatedly emerged. Therefore, using laser techniques to control the field-free molecular alignment and orientation in a non-adiabatic regime is more valuable for real applications.

So far, dynamical analysis of alignment and orientation driven by linearly polarized laser pulses for linear molecules has been widely studied both experimentally and theoretically. By contrast, the field-free molecular alignment and orientation of linear molecules induced by elliptically polarized laser pulses are relatively rarely discussed. In recent years, some of the alignment and orientation induced by elliptically polarized laser pulses have been reported. For example, Daems *et al.*<sup>[28]</sup> and Hertz *et al.*<sup>[29]</sup> have used elliptically polarized laser pulses to achieve three-dimensional (3D) field-free molecular alignment and shown a different quantum process. Maan *et al.*<sup>[30]</sup> have achieved field-free molecular orientation by delayed elliptically polarized laser pulses and analyzed the effect of pulse parameters on the rotational excitation and orientation dynamics; however, they only selected one direction to discuss. Due to the different properties from linearly polarized laser pulses, molecular alignment and orientation by elliptically polarized laser pulses have become an interesting topic.

In this Letter, we use the density matrix method to study the molecular alignment and orientation driven by two elliptically polarized laser pulses. We describe the full Hamiltonian of the system and the numerical calculation method in detail. We compare the alignment and orientation results steered by the elliptically polarized laser pulse, and analyze the populations of the rotational states after the laser pulse. Then, the effects of the delay time and elliptic parameters on alignment and orientation are discussed. Finally, the conclusions are drawn.

In this work, the two elliptically polarized laser pulses  $E(t)$  used can be written as<sup>[29,30]</sup>

$$\vec{E}_i(t) = E_0(t) \{ \vec{e}_x a_i \cos[\omega_i(t - t_i)] + \vec{e}_y b_i \sin[\omega_i(t - t_i)] \}, \quad (i = 1, 2), \quad (1)$$

with

$$E_0(t) = E_i \exp[-(t - t_i)^2 / 2\sigma_i^2], \quad (2)$$

where  $E_i$  denotes the electric field intensity,  $\omega_i$  is the field frequency,  $a_i$  and  $b_i$  represent the half-axis of the ellipse along the  $x$  and  $y$  axes, respectively, with  $a_i^2 + b_i^2 = 1$ ,  $t_i$  is the pulse center time, and  $\sigma_i$  is the pulse half-duration. The delay time between the two elliptically polarized laser pulses is  $t_2 - t_1$ . Based on the rigid-rotor model, the Hamiltonian for this system is

$$\hat{H}_0(t) = \hat{H}_0 + \hat{H}_{\text{pol}}(t) + \hat{H}_{\text{dip}}(t). \quad (3)$$

Here the first term  $\hat{H}_0 = B_e \hat{J}^2$  is the molecular rotation energy, in which  $B_e$  denotes the molecular rotational constant and  $\hat{J}$  the angular momentum operator. The second term is the polarization interaction between the elliptically polarized laser pulse and the molecule, which can be described as

$$\hat{H}_{\text{pol}}(t) = -\frac{1}{4} E_0^2(t) (\alpha_{\parallel} - \alpha_{\perp}) \sin^2 \theta [(a_1^2 - b_1^2) \cos^2 \phi + b_1^2], \quad (4)$$

in which  $\alpha_{\parallel}$  and  $\alpha_{\perp}$  are the polarizabilities parallel and perpendicular to the molecular axis, respectively,  $\theta$  is the angle between the molecular axis and  $z$  axis, which is orthogonal to the ellipse plane, and  $\phi$  is the azimuthal angles along the  $z$  axis. The last term means the dipole interaction, which can be read as

$$\hat{H}_{\text{dip}}(t) = -\mu E_0(t) a_2 \sin \theta \cos \phi \cos[\omega_2(t - t_2)] + \mu E_0(t) b_2 \sin \theta \sin \phi \sin[\omega_2(t - t_2)], \quad (5)$$

with  $\mu$  being the permanent dipole moment.

The time evolution of the density operator is obtained by solving the Liouville equation,

$$\frac{d\hat{\rho}(t)}{dt} = -\frac{i}{\hbar} [\hat{H}, \hat{\rho}(t)]. \quad (6)$$

If the eigenvector of the Hamiltonian is expressed by  $|JM\rangle$ , then  $\hat{\rho}(t)$  can be expanded as  $\hat{\rho}(t) = \sum_{JM, J'M'} \rho_{JM, J'M'}(t) |JM\rangle \langle J'M'|$ , where the matrix elements  $\rho_{JM, J'M'}(t)$  are given by solving the coupling equation<sup>[31]</sup>:

$$\begin{aligned} \frac{d\rho_{JM, J'M'}(t)}{dt} = & -\frac{i}{\hbar} \left\{ \sum_{J_1 M_1} (\rho_{J_1 M_1, J'M'}(t) \langle JM | B_e \hat{J}^2 | J_1 M_1 \rangle \right. \\ & - \rho_{JM, J_1 M_1}(t) \langle J_1 M_1 | B_e \hat{J}^2 | J'M' \rangle) \\ & - \frac{1}{4} E_0^2(t) (\alpha_{\parallel} - \alpha_{\perp}) \sum_{J_1 M_1} [(a_1^2 - b_1^2) (\rho_{J_1 M_1, J'M'}(t) \\ & \cdot \langle JM | \sin^2 \theta \cos^2 \phi | J_1 M_1 \rangle \\ & - \rho_{JM, J_1 M_1}(t) \langle J_1 M_1 | \sin^2 \theta \cos^2 \phi | J'M' \rangle)] \\ & - b_1^2 (\rho_{J_1 M_1, J'M'}(t) \langle JM | \cos^2 \theta | J_1 M_1 \rangle \\ & - \rho_{JM, J_1 M_1}(t) \langle J_1 M_1 | \cos^2 \theta | J'M' \rangle) \\ & - \mu E_0(t) \sum_{J_1 M_1} [a_2 \cos(\omega_2(t - t_2)) (\rho_{J_1 M_1, J'M'}(t) \\ & \cdot \langle JM | \sin \theta \cos \phi | J_1 M_1 \rangle \\ & - \rho_{JM, J_1 M_1}(t) \langle J_1 M_1 | \sin \theta \cos \phi | J'M' \rangle) \\ & + b_2 \sin(\omega_2(t - t_2)) (\rho(t) \\ & \cdot \langle JM | \sin \theta \sin \phi | J_1 M_1 \rangle \\ & - \rho_{JM, J_1 M_1}(t) \langle J_1 M_1 | \sin \theta \sin \phi | J'M' \rangle)] \left. \right\}. \quad (7) \end{aligned}$$

In the representation of angular momentum, the initial density operator is a diagonal matrix, which satisfies the temperature-dependent Boltzmann distribution:

$$\rho_0(T) = \frac{1}{Z} \sum_{J=0}^{\infty} \sum_{M=-J}^M |JM\rangle \langle JM| e^{-\varepsilon / K_B T}, \quad (8)$$

where  $\varepsilon = B_e J(J + 1)$  is the molecular rotational energy of the  $|JM\rangle$  state,  $Z = \sum_{J=0}^{\infty} \sum_{M=-J}^M e^{-\varepsilon / K_B T}$  is the partition function with the Boltzmann constant  $K_B$  at temperature  $T$ . The molecular alignment and orientation degrees along the three axes are<sup>[32]</sup>

$$\left. \begin{aligned} \langle \cos^2 \theta_x \rangle &= Tr\{\sin^2 \theta \cos^2 \phi \hat{\rho}(t)\} \\ \langle \cos^2 \theta_y \rangle &= Tr\{\sin^2 \theta \sin^2 \phi \hat{\rho}(t)\} \\ \langle \cos^2 \theta_z \rangle &= Tr\{\cos^2 \theta \hat{\rho}(t)\} \end{aligned} \right\}, \quad (9)$$

$$\left. \begin{aligned} \langle \cos \theta_x \rangle &= Tr\{\sin \theta \cos \phi \hat{\rho}(t)\} \\ \langle \cos \theta_y \rangle &= Tr\{\sin \theta \sin \phi \hat{\rho}(t)\} \\ \langle \cos \theta_z \rangle &= Tr\{\cos \theta \hat{\rho}(t)\} \end{aligned} \right\}. \quad (10)$$

The CO molecule is taken as an example to analyze its alignment and orientation dynamics. The molecular parameters are as follows:  $B_e = 1.93 \text{ cm}^{-1}$ ,  $\mu = 0.112 \text{ D}$ ,  $\alpha_{\parallel} = 2.294 \text{ \AA}^3$  ( $1 \text{ \AA} = 0.1 \text{ nm}$ ),  $\alpha_{\perp} = 1.77 \text{ \AA}^3$ <sup>[33]</sup>. The rotational period  $T_{\text{rot}} = h/2B_e = 8.64 \text{ ps}$  and the temperature of the system is taken to be  $T = 0 \text{ K}$ . Here, we use two elliptically polarized laser pulses with different frequencies to interact with molecules. The first pulse with frequency  $12,500 \text{ cm}^{-1}$  is used to align the molecule, and the second pulse with THz frequency is added to orient the molecule. Figures [1\(a\)](#) and [1\(b\)](#) show the time evolutions of the

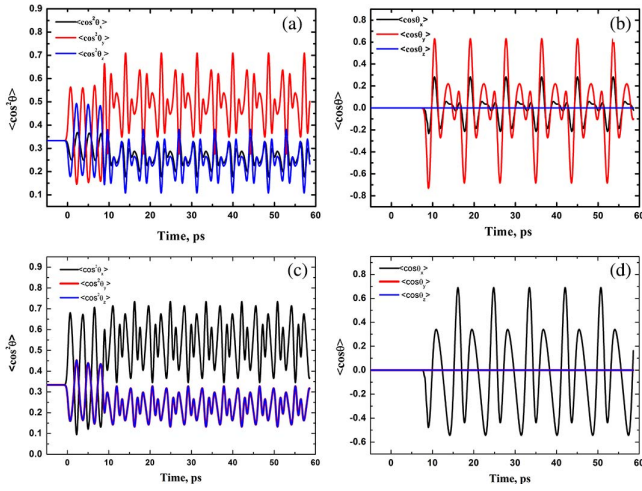


Fig. 1. Time evolutions of field-free molecular (a) alignment and (b) orientation along the three axes steered by the elliptically polarized laser pulse with  $E_1 = 5.0 \times 10^7$  V/cm,  $E_2 = 4.0 \times 10^7$  V/cm,  $\omega_1 = 12,500$  cm $^{-1}$ ,  $\omega_2 = 36$  cm $^{-1}$ ,  $\sigma_1 = 0.4$  ps,  $\sigma_2 = 0.45$  ps,  $a_1 = a_2 = 0.5$ ,  $t_1 = 0$ , and  $t_2 = 1T_{\text{rot}}$ . The time evolutions of field-free molecular (c) alignment and (d) orientation steered by the linearly polarized laser pulses with  $a_1 = a_2 = 1.0$ , while the other parameters are the same as those in (a) and (b).

field-free molecular alignment and orientation along three axes driven by elliptically polarized laser pulses, respectively. It can be seen from Fig. 1(a) that in a non-adiabatic regime, the 3D field-free molecular alignment can be achieved. After the laser pulse, the maximum of  $\langle \cos^2 \theta_y \rangle$  appears periodically at around  $T = \frac{1}{2}nT_{\text{rot}}$  ( $n = 1, 3, 5, \dots$ ), while the maximum of  $\langle \cos^2 \theta_x \rangle$  and  $\langle \cos^2 \theta_z \rangle$  appears regularly at around  $nT_{\text{rot}}$  ( $n = 1, 2, 3, \dots$ ). At any time, the alignment degrees of these three axes satisfy the equation  $\sum_{i=x,y,z} \langle \cos^2 \theta_i \rangle(t) = 1$ <sup>[28]</sup>. Based on this principle, if we know the alignment results of any two axes, the alignment degrees on the third axis can be deduced. Compared with the 3D field-free alignment results, the field-free molecular orientation by elliptically polarized laser pulses is very different. It should be pointed out that a molecule cannot be oriented along the  $z$  axis (orthogonal to the polarized plane), i.e., we can only obtain a two-dimensional (2D) field-free orientation along the  $x$  and  $y$  directions. Moreover, as shown in Fig. 1(b),  $\langle \cos \theta_x \rangle$  and  $\langle \cos \theta_y \rangle$  appear periodically at around  $T = nT_{\text{rot}}$  ( $n = 1, 2, 3, \dots$ ). In comparison, Figs. 1(c) and 1(d) show the time evolutions of field-free alignment and orientation driven by linear laser pulses. It can be seen from Fig. 1(c) that although the 3D alignment results can be obtained, the alignment mainly along the  $x$  direction, i.e., the pulse polarization direction, and the other two directions have lower alignment degrees. In addition, from Fig. 1(d), we can see that the molecule cannot be oriented along the  $y$  and  $z$  axes; instead, it only exists on the  $x$  axis. Due to the alternation of two-direction alignment and orientation driven by elliptically polarized laser pulses, this technique is more useful for some real applications, such as the 3D molecular switch.

In order to track the physical origin of the above alignment and orientation by the elliptically polarized laser pulses, we further give the populations of each rotational state after the laser pulse in Fig. 2. In this system, molecules excited from the initial state ( $|00\rangle$ ) undergo two kinds of interaction. One is the anisotropic polarizability interaction, under which the transition matrix element  $\langle J_1 M_1 | \cos^2 \theta | J M \rangle$  follows the selection rules of  $\Delta J = 0, \pm 2$ ,  $\Delta M = 0$ , and  $\langle J_1 M_1 | \sin^2 \theta \cos^2 \phi | J M \rangle$  follows the selection rules of  $\Delta J = 0, \pm 2$ ,  $\Delta M = 0, \pm 2$ , leading to the molecule being populated on even states. The other is called the permanent dipole interaction, under which the transition matrix elements  $\langle J_1 M_1 | \sin \theta \cos \phi | J M \rangle$  and  $\langle J_1 M_1 | \sin \theta \sin \phi | J M \rangle$  in Eq. (10) follow the selection rules of  $\Delta J = \pm 1$ ,  $\Delta M = \pm 1$ , leading to the populations being on odd states, which results in the appearance of orientations. Based on the above different selection rules, there are no populations on  $|1, 0\rangle$ ,  $|2, -1\rangle$ ,  $|2, 1\rangle$ ,  $|3, 0\rangle$ ,  $|3, -2\rangle$ , and  $|3, 2\rangle$  states, as shown in Fig. 2. According to Eq. (10),  $\langle \cos \theta_z \rangle$  is related to the matrix element  $\langle J_1 M_1 | \cos \theta | J M \rangle$ , which follows the selection rules of  $\Delta J = \pm 1$ ,  $\Delta M = 0$ , i.e., the populations on  $|1, 0\rangle$  and  $|3, 0\rangle$  states are required. However, this case cannot be achieved by elliptically polarized laser pulses, and eventually, only 2D field-free orientation can be obtained. It can be deduced that the magnetic quantum numbers play an important role in the field-free alignments and orientations along different axes. Moreover, the results indicate that as long as the  $|J, 0\rangle$  state has a proper distribution, an efficient orientation degree along the  $z$  axis can be obtained.

To display the impact of delay time on field-free molecular alignment and orientation, the maximal alignment degrees  $\langle \cos^2 \theta \rangle_{\text{max}}$  and the maximal orientation degrees  $\langle \cos \theta \rangle_{\text{max}}$  as a function of the delay time are shown in Fig. 3. It can be seen that every curve shows irregular oscillations, and the maximal value of  $\langle \cos^2 \theta_x \rangle_{\text{max}}$  and  $\langle \cos \theta_x \rangle_{\text{max}}$  occurs at  $0.7T_{\text{rot}}$ . For  $\langle \cos^2 \theta_y \rangle_{\text{max}}$  and  $\langle \cos \theta_y \rangle_{\text{max}}$ , the highest value occurs at  $0.3T_{\text{rot}}$ , while for  $\langle \cos^2 \theta_z \rangle_{\text{max}}$ , the highest value appears at  $0.9T_{\text{rot}}$ .

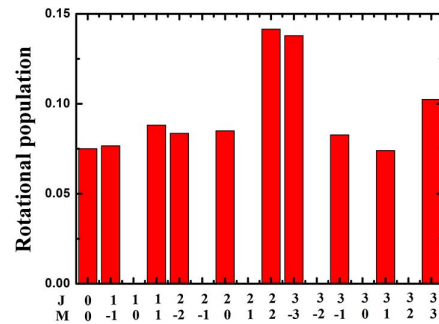


Fig. 2. Populations of rotational states after the elliptically polarized laser pulse with  $E_1 = 5.0 \times 10^7$  V/cm,  $E_2 = 4.0 \times 10^7$  V/cm,  $\omega_1 = 12,500$  cm $^{-1}$ ,  $\omega_2 = 36$  cm $^{-1}$ ,  $\sigma_1 = 0.4$  ps,  $\sigma_2 = 0.45$  ps,  $a_1 = a_2 = 0.5$ ,  $t_1 = 0$ , and  $t_2 = 1T_{\text{rot}}$ .

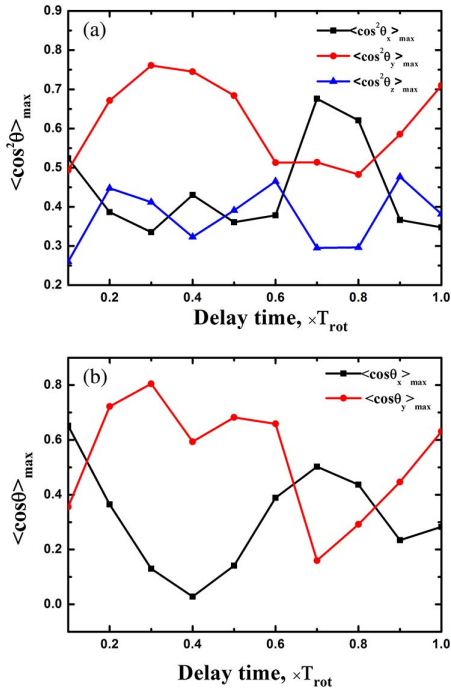


Fig. 3. (a) Maximum of alignment  $\langle \cos^2 \theta \rangle_{\max}$  and (b) orientation  $\langle \cos \theta \rangle_{\max}$  as a function of delay time with  $E_1 = 5.0 \times 10^7$  V/cm,  $E_2 = 4.0 \times 10^7$  V/cm,  $\omega_1 = 12,500$  cm<sup>-1</sup>,  $\omega_2 = 36$  cm<sup>-1</sup>,  $\sigma_1 = 0.4$  ps,  $\sigma_2 = 0.45$  ps,  $a_1 = a_2 = 0.5$ .

Just as we know that the interference effect of the rotational states can make the molecule reacquire the spatial alignment and orientation, when the highest value is achieved, it presents a constructive interference; on the contrary, it indicates a destructive interference. So changing the delay time between these two elliptically polarized laser pulses can control the field-free molecular alignment and orientation.

To further explore the field-free molecular alignment and orientation by the elliptically polarized laser pulses, we calculate the maximum degrees of alignment  $\langle \cos^2 \theta \rangle_{\max}$  and the maximum degrees of orientation  $\langle \cos \theta \rangle_{\max}$  with the changing elliptic parameters, and the results are shown in Fig. 4. Figure 4(a) presents the maximum alignment degree  $\langle \cos^2 \theta \rangle_{\max}$  as a function of the elliptic parameter  $a_1$  driven by the initial elliptically polarized laser pulse. From it, we can find that when  $a_1 = 0$  and 1, which means a linearly polarized laser pulse along the  $y$  and  $x$  axes, respectively, the highest value of  $\langle \cos^2 \theta_y \rangle_{\max}$  and  $\langle \cos^2 \theta_x \rangle_{\max}$  can be obtained. In addition, when  $\langle \cos^2 \theta_x \rangle_{\max}$  or  $\langle \cos^2 \theta_y \rangle_{\max}$  achieves the highest value, the maximum alignment degrees of another two axes are equal. It is worth noting that in the near circular polarization case, i.e.,  $a_1 = 0.7$ , the maximum alignment along the  $z$  axis  $\langle \cos^2 \theta_z \rangle_{\max}$  is largest, while the maximum degrees of  $\langle \cos^2 \theta_y \rangle_{\max}$  and  $\langle \cos^2 \theta_x \rangle_{\max}$  are equal. From Fig. 4(a), we also notice that  $\langle \cos^2 \theta_y \rangle_{\max}$  has a minimum value at  $a_1 = 0.6$ , and  $\langle \cos^2 \theta_x \rangle_{\max}$  gets the minimum value at  $a_1 = 0.8$ . A reasonable explanation is that the

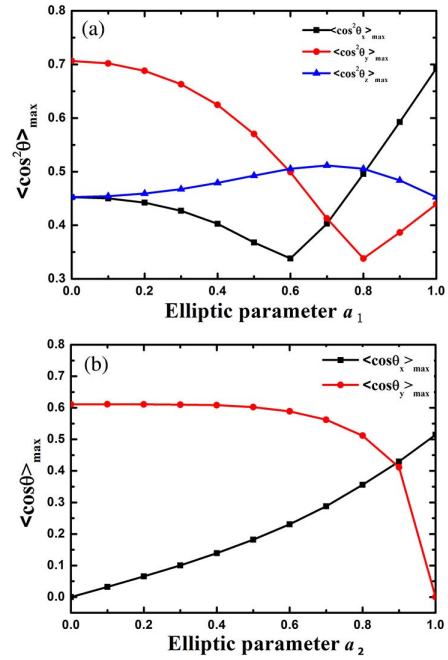


Fig. 4. (a) Plots of the maximal alignment degrees along three axes versus the elliptic parameter  $a_1$  with  $E_1 = 5.0 \times 10^7$  V/cm,  $\omega_1 = 12,500$  cm<sup>-1</sup>,  $\sigma_1 = 0.4$  ps, and  $t_1 = 0$ . (b) Plots of the maximal orientation degrees versus the elliptic parameter  $a_2$ , with  $E_1 = 5.0 \times 10^7$  V/cm,  $E_2 = 4.0 \times 10^7$  V/cm,  $\omega_1 = 12,500$  cm<sup>-1</sup>,  $\omega_2 = 36$  cm<sup>-1</sup>,  $\sigma_1 = 0.4$  ps,  $\sigma_2 = 0.45$  ps,  $a_1 = 0.7$ ,  $t_1 = 0$ , and  $t_2 = 1T_{\text{rot}}$ .

elliptically polarized laser pulse with the parameters  $a$  and  $b$  can be written as a superposition of two linearly polarized laser pulses along the  $x$  and  $y$  axes<sup>[29,34]</sup>. Thus,  $\langle \cos^2 \theta_x \rangle_{a^2}(t)$  and  $\langle \cos^2 \theta_y \rangle_{a^2}(t)$  are considered as the combination of the effects of the two axes, which follow the equations:

$$\langle \cos^2 \theta_y \rangle_{a^2}(t) \approx b^2 y_1 + a^2 x_1 = \left( \frac{1-3a^2}{2} \right) y_1 + \frac{a^2}{2}, \quad (11)$$

$$\langle \cos^2 \theta_x \rangle_{a^2}(t) \approx a^2 y_1 + b^2 x_1 = \left( \frac{3a^2-1}{2} \right) y_1 - \frac{a^2}{2} + \frac{1}{2}, \quad (12)$$

where  $y_1 = \langle \cos^2 \theta_y \rangle_{a^2=0}(t)$  is the alignment along the  $y$  axis at  $a^2 = 0$ ,  $x_1 = \langle \cos^2 \theta_x \rangle_{a^2=0}(t)$  is the alignment along the  $x$  axis at  $a^2 = 0$ , and  $\langle \cos^2 \theta_x \rangle_{a^2=0}(t) = \langle \cos^2 \theta_z \rangle_{a^2=0}(t)$ . Using the principle  $\sum_{i=x,y,z} \langle \cos^2 \theta_i \rangle(t) = 1$ , it can be obtained that  $\langle \cos^2 \theta_x \rangle_{a^2=0}(t) = \frac{1}{2}[1 - \langle \cos^2 \theta_y \rangle_{a^2=0}(t)]$ , i.e.,  $x_1 = \frac{(1-y_1)}{2}$ . According to Eqs. (11) and (12), when  $a^2 = \frac{1}{3}$ ,  $\langle \cos^2 \theta_y \rangle_{a^2=0}(t)$  has a maximum value, and when  $a^2 = \frac{2}{3}$ , the highest value appears for  $\langle \cos^2 \theta_y \rangle_{a^2=0}(t)$ , which corresponds roughly to  $a_1 = 0.6$  and  $a_1 = 0.8$ , respectively, as reflected in Fig. 4(a).

Figure 4(b) shows the maximum orientation degrees  $\langle \cos \theta_x \rangle_{\max}$  and  $\langle \cos \theta_y \rangle_{\max}$  as a function of the elliptic

parameter  $a_2$  driven by the combined elliptically polarized laser pulses. It is found that  $\langle \cos \theta_x \rangle_{\max}$  presents a monotonical increase with  $a_2$  changing from 0 to 1, while  $\langle \cos \theta_y \rangle_{\max}$  decreases slowly at first and then decreases rapidly with the increase of  $a_2$ . When  $a_2 = 0.9$ ,  $\langle \cos \theta_x \rangle_{\max}$  and  $\langle \cos \theta_y \rangle_{\max}$  are approximately the same, which indicates that the coherent effects of the rotational wave packet on the  $x$  and  $y$  axes are the same.

The above analyses are under the non-adiabatic regime. To study the in-pulse molecular alignment and orientation induced by the elliptically polarized laser pulses, the time evolutions of 3D alignments driven by the initial elliptically polarized laser pulse with different elliptic parameter  $a_1$  and 2D orientations driven by the combined elliptically polarized laser pulses with a different elliptic parameter  $a_2$  are shown in Fig. 5. It can be seen from Figs. 5(a)–5(e) that due to the average thermal distribution, the alignment degrees on three axes are equal before and after being driven by the laser pulse. The in-pulse alignments of  $\langle \cos^2 \theta_x \rangle$  and  $\langle \cos^2 \theta_y \rangle$  show an opposite changing pattern with the increase of  $a_1$ . For  $\langle \cos^2 \theta_x \rangle$ , with  $a_1$  increasing from 0.5 to 0.9, the overall oscillation pattern changes from valley to peak gradually. This is because with  $a_1$  increasing, the field intensity on the  $x$  axis gradually increases and, hence, improves the alignment in the  $x$  direction. For  $\langle \cos^2 \theta_y \rangle$ , an opposite situation arises, i.e., when  $a_1$  increases from 0.5 to 0.9, the alignment in the  $y$  direction is gradually inhibited. However, because there is no

field intensity in the  $z$  direction, the in-pulse alignment of  $\langle \cos^2 \theta_z \rangle$  does not change with the increase of  $a_1$ . Therefore, in combination with Figs. 1, 3, 4, and 5(a)–5(e), we can infer that the field-free molecular alignment on the  $z$  axis depends on the interference effect of specific populated rotational states. Choosing the different delay time, the elliptic parameter and other parameters can change the population of rotational states, impacting the molecular alignment. For the in-pulse alignment, the interaction between the molecules and the laser field creates a pendular state, which evolves along with the polarization vector. The maximum degree of the molecular alignment reached during the interaction is related to the field intensity distribution on different axes rather than the periodic dephasing and rephasing of the rotational wave packet. So the alignment on the  $x$  and  $y$  directions shows an alternate changing pattern, while the alignment on the  $z$  axis does not change with the elliptic parameter. To study the in-pulse orientations, the second elliptically polarized laser pulse is added after  $2T_{\text{rot}}$ . Compared with the pure adiabatic 3D alignments, the 2D orientation shown in Figs. 5(f)–5(j) corresponds to an intermediate regime between non-adiabatic and adiabatic regimes. It can be seen that with  $a_2$  increasing from 0.5 to 0.9, the maximum of  $|\langle \cos \theta_x \rangle|$  increases gradually; meanwhile, the maximum of  $\langle \cos \theta_y \rangle$  decreases gradually. This phenomenon can also be explained by the different field distributions on the  $x$  and  $y$  axes.

We have theoretically studied the molecular alignment and orientation induced by elliptically polarized laser pulses. It is shown that the 3D field-free molecular alignment can be achieved by elliptically polarized laser pulses, while the field-free orientation can only be realized along the  $x$  and  $y$  directions. From the populations of each rotational state with different magnetic quantum numbers after the laser pulse, we can deduce that the lack of a  $|J, 0\rangle$  state leads to molecules not being oriented along the  $z$  axis. By choosing an appropriate delay time, the field-free alignment and orientation degree can be enhanced. Also shown is that the field-free alignment by one elliptically polarized laser pulse can be seen as a superposition of alignment by two linearly polarized laser pulses along the  $x$  and  $y$  axes. In addition, for the in-pulse alignment and orientation, changing the elliptic parameters only influences the alignment and orientation results in the  $x$  and  $y$  directions, from which it can be inferred that it is the field intensity distribution on the  $x$  and  $y$  axes rather than the periodic dephasing and rephasing of the rotational wave packet that gives rise to the in-pulse alignment and orientation. The above conclusions are significant for the external manipulation of molecular field-free alignment and orientation.

This work was supported by the National Natural Science Foundation of China (No. 11674198) and the Taishan Scholar Project of Shandong Province.

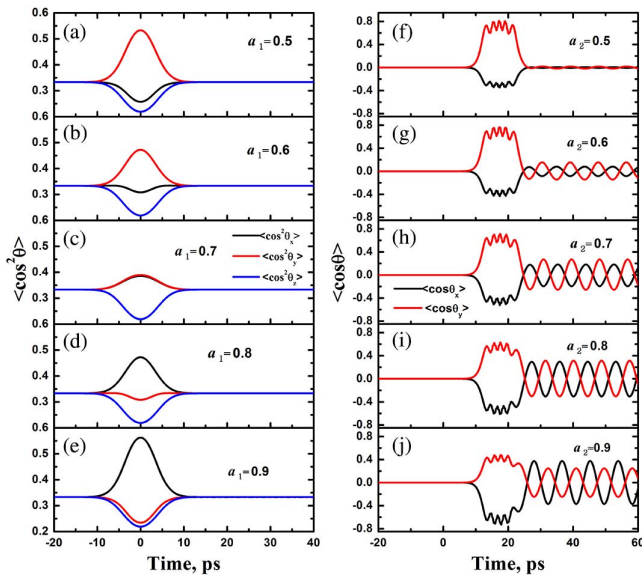


Fig. 5. (a)–(e) Time evolutions of 3D alignments with different elliptic parameters  $a_1$  driven by the initial elliptically polarized laser pulse with  $\sigma_1 = 5$  ps,  $E_1 = 5.0 \times 10^7$  V/cm,  $\omega_1 = 12,500$  cm $^{-1}$ , and  $t_1 = 0$ . (f)–(j) Time evolutions of 2D orientations with different elliptic parameters  $a_2$  steered by two elliptically polarized laser pulses with  $E_1 = 5.0 \times 10^7$  V/cm,  $E_2 = 4.0 \times 10^7$  V/cm,  $\omega_1 = 12,500$  cm $^{-1}$ ,  $\omega_2 = 36$  cm $^{-1}$ ,  $\sigma_1 = 5$  ps,  $\sigma_2 = 3$  ps,  $a_1 = 0.7$ ,  $t_1 = 0$ , and  $t_2 = 2T_{\text{rot}}$ .

## References

1. T. Seideman, *J. Chem. Phys.* **113**, 1677 (2000).
2. J. Hu, K. L. Han, and G. Z. He, *Phys. Rev. Lett.* **95**, 123001 (2005).
3. T. Suzuki, S. Minemoto, T. Kanai, and H. Sakai, *Phys. Rev. Lett.* **92**, 133005 (2004).
4. T. Kanai, S. Minemoto, and H. Sakai, *Nature* **435**, 470 (2005).
5. T. Kanai, S. Minemoto, and H. Sakai, *Phys. Rev. Lett.* **98**, 053002 (2007).
6. H. Wu, S. Yue, J. Li, S. Fu, B. Hu, and H. Du, *Chin. Opt. Lett.* **16**, 040203 (2018).
7. M. Li, G. Zhang, T. Zhao, X. Ding, and J. Yao, *Chin. Opt. Lett.* **15**, 120202 (2017).
8. H. Ohmura, N. Saito, and M. Tachiya, *Phys. Rev. Lett.* **96**, 173001 (2006).
9. H. Stapelfeldt and T. Seideman, *Rev. Mod. Phys.* **75**, 543 (2003).
10. Y. Niu and R. Wang, *Chin. Opt. Lett.* **16**, 060201 (2018).
11. D. H. Parker and R. B. Bernstein, *Ann. Rev. Phys. Chem.* **40**, 561 (1989).
12. T. D. Hain, R. M. Moision, and T. J. Curtiss, *J. Chem. Phys.* **111**, 6797 (1999).
13. L. Cai, J. Marango, and B. Friedrich, *Phys. Rev. Lett.* **86**, 775 (2001).
14. S. A. Zhang, C. H. Lu, T. Q. Jia, Z. G. Wang, and Z. R. Sun, *J. Chem. Phys.* **135**, 034301 (2011).
15. J. Wu and H. P. Zeng, *Phys. Rev. A* **81**, 053401 (2010).
16. M. Muramatsu, M. Hita, S. Minemoto, and H. Sakai, *Phys. Rev. A* **79**, 011403 (2009).
17. S. A. Zhang, C. H. Lu, T. Q. Jia, Z. G. Wang, and Z. R. Sun, *Phys. Rev. A* **83**, 043410 (2011).
18. S. L. Liao, T. S. Ho, H. Rabitz, and S. I. Chu, *Phys. Rev. A* **87**, 013429 (2013).
19. S. Fleischer, Y. Zhou, R. W. Field, and K. A. Nelson, *Phys. Rev. Lett.* **107**, 163603 (2011).
20. C. C. Qin, Y. Tang, Y. M. Wang, and B. Zhang, *Phys. Rev. A* **85**, 053415 (2012).
21. C. C. Shu, K. J. Yuan, W. H. Hu, and S. L. Cong, *Opt. Lett.* **34**, 3190 (2009).
22. H. Li, X. W. Li, Y. H. Feng, H. F. Pan, and H. P. Zeng, *Phys. Rev. A* **88**, 013424 (2013).
23. Y. Huang, T. Xie, J. Li, J. Yu, and S. L. Cong, *Laser Phys.* **24**, 016002 (2014).
24. Y. Liu, J. Li, J. Yu, and S. L. Cong, *Laser Phys. Lett.* **10**, 076001 (2013).
25. R. Torres, R. de. Nalda, and J. P. Marangos, *Phys. Rev. A* **72**, 023420 (2005).
26. Q. Y. Cheng, J. S. Liu, D. G. Yue, X. C. Zhou, and Q. T. Meng, *J. Phys. B: At. Mol. Opt. Phys.* **51**, 065401 (2018).
27. F. Rosca-Pruna and M. J. J. Vrakking, *Phys. Rev. Lett.* **87**, 153902 (2001).
28. D. Daems, S. Guerin, E. Hertz, H. R. Jauslin, B. Lavorel, and O. Faucher, *Phys. Rev. Lett.* **95**, 063005 (2005).
29. E. Hertz, A. Rouzee, S. Guerin, B. Lavorel, and O. Faucher, *Phys. Rev. A* **76**, 043423 (2007).
30. A. Maan, A. Tyagi, and V. Prasad, *Spectrochim Acta A* **188**, 268 (2018).
31. J. S. Liu, Q. Y. Cheng, D. G. Yue, X. C. Zhou, and Q. T. Meng, *Chin. Phys. B* **27**, 033301 (2018).
32. S. Ramakrishna and T. Seideman, *J. Chem. Phys.* **124**, 034101 (2006).
33. K. A. Peterson and T. H. Dunning, *J. Mol. Struct-Theochem.* **400**, 93 (1997).
34. A. Rouzee, S. Guerin, F. Faucher, and B. Lavorel, *Phys. Rev. A* **77**, 043412 (2008).